Oxygen-enhanced MRI detects incidence, onset and heterogeneity of radiation-induced hypoxia modification in HPV-associated oropharyngeal cancer

DOI:
10.1158/1078-0432.CCR-24-1170

Document Version
Accepted author manuscript

Citation for published version (APA):
Dubec, M., Price, J., Berks, M., Gaffney, J., Little, R., Porta, N., Sridharan, N., Datta, A., McHugh, D., Hague, C., Cheung, S., Manoharan, P., Van Herk, M., Choudhury, A., Matthews, J., Parker, G., Buckley, D., Harrington , K. J., Mcpartlin, A., & O'Connor, J. (2024). Oxygen-enhanced MRI detects incidence, onset and heterogeneity of radiation-induced hypoxia modification in HPV-associated oropharyngeal cancer. *Clinical Cancer Research*. Advance online publication. https://doi.org/10.1158/1078-0432.CCR-24-1170

Published in:
Clinical Cancer Research

Oxygen-enhanced MRI detects incidence, onset and heterogeneity of radiation-induced hypoxia modification in HPV-associated oropharyngeal cancer

Michael J Dubec[1,2], James Price[3], Michael Berks[1], John Gaffney[3], Ross A Little[1], Nuria Porta[4], Nivetha Sridharan[4], Anubhav Datta[1,5], Damien J McHugh[1,2], Christina J Hague[3], Susan Cheung[1], Prakash Manoharan[5], Marcel van Herk[1], Ananya Choudhury[1,3], Julian C Matthews[6], Geoff JM Parker[7,8], David L Buckley[2,9], Kevin J Harrington[10], Andrew McPartlin[3,11], James PB O'Connor[1,5,10]

[1]Division of Cancer Sciences, University of Manchester, Manchester

[2]Christie Medical Physics and Engineering, The Christie NHS Foundation Trust, Manchester

[3]Clinical Oncology, The Christie NHS Foundation Trust, Manchester

[4]Clinical Trials and Statistics Unit, The Institute of Cancer Research, London

[5]Radiology Department, The Christie NHS Foundation Trust, Manchester

[6]Psychology, Communication & Human Neuroscience, University of Manchester, Manchester

[7]Bioxydyn Ltd, Manchester

[8]Centre for Medical Image Computing, Department of Medical Physics and Biomedical Engineering, University College London, London

[9]Biomedical Imaging, University of Leeds, Leeds

[10]Division of Radiotherapy and Imaging, The Institute of Cancer Research, London

[11]Radiation Oncology, Princess Margaret Cancer Center, Toronto

Corresponding author

Michael J Dubec, Christie Medical Physics and Engineering, The Christie NHS Foundation Trust, Wilmslow Road, Manchester, M20 4BX, United Kingdom.

michael.dubec@nhs.net

Running Title

Oxygen-enhanced MRI in HPV-associated oropharyngeal cancer

Conflict of Interest Statement

Geoff JM Parker is an employee of and holds ownership interest (including patents) in Bioxydyn Limited. All other authors declare no potential conflicts of interest.

Statement of Translational Relevance

Tumor hypoxia reduces the effectiveness of radiotherapy, chemotherapy, and immunotherapy, leading to poorer outcomes. Recent studies have suggested that patients with HPV-associated oropharyngeal carcinoma may benefit from radiation dose de-escalation guided by the persistence of hypoxia. We show here that oxygen-enhanced (OE)-MRI can map the variable onset and duration of radiotherapy-induced hypoxia modification, demonstrating that early scanning could identify which patients will benefit from dose de-escalation. Half of all patients with both a primary and nodal tumor had discordant hypoxia modification where only one lesion changed with therapy, emphasizing that personalized therapeutic approaches should consider all measurable disease rather than one target lesion. Hypoxic volumes were not simple surrogates of overall tumor volume, confirming the value of measuring hypoxia as an outcome variable. Collectively, these data support using OE-MRI in larger studies to evaluate dose de-escalation.

Abstract

Background: Hypoxia mediates treatment resistance in solid tumors. We evaluated if oxygen-enhanced (OE)-MRI-derived hypoxic volume (HV_{MRI}) is repeatable and can detect radiotherapy-induced hypoxia modification in HPV-associated oropharyngeal head and neck squamous cell cancer (HNSCC).

Patients and Methods: 27 patients were recruited prospectively between March 2021 and January 2024. HV_{MRI} was measured in primary and nodal tumors prior to standard-of-care (chemo)radiotherapy then at weeks 2 and 4 (W2, W4) into therapy. Two pre-treatment scans assessed biomarker within-subject coefficient of variation (wCV) and repeatability coefficient (RC). Cohort treatment response was measured using mixed-effects modelling. Responding lesions were identified by comparing HV_{MRI} change to RC limits of agreement (LOA).

Results: OE-MRI identified hypoxia in all lesions. HV_{MRI} wCV was 24.6% and RC LOA were -45.7% to 84.1%. Cohort median pre-treatment HV_{MRI} of 11.3 cm^3 reduced to 6.9 cm^3 at W2 and 5.9 cm^3 at W4 (both $p < 0.001$). HV_{MRI} was reduced in 54.5% of individual lesions by W2 and in 88.2% by W4. All lesions with W2 hypoxia reduction showed persistent modification at W4. HV_{MRI} reduced in some lesions that showed no overall volume change. Hypoxia modification was discordant between primary and nodal tumors in 50.0% of patients.

Conclusions: Radiation-induced hypoxia modification can occur as early as W2, but onset varies between patients and was not necessarily associated with overall size change. Half of all patients had discordant changes in primary and nodal tumors. These findings have implications for patient selection and timing of dose de-escalation strategies in HPV-associated oropharyngeal carcinoma.

Introduction

Hypoxia is a feature of nearly all solid tumors, including head and neck squamous cell carcinoma (HNSCC) (1). The presence and extent of hypoxia indicates both poor prognosis and resistance to radiotherapy (2), chemotherapy (3), targeted therapies, and immunotherapy (4). Imaging can be used to identify whether patients have hypoxic tumors prior to therapy, and to quantify the extent, spatial and temporal variation of hypoxia (5). This has the potential to assist adaptive radiotherapy. Specifically, there is evidence that identifying hypoxia modification early in therapy can guide dose de-escalation in patients with human papillomavirus (HPV)-associated oropharyngeal carcinoma (OPC) (6-8) to reduce normal tissue toxicity, or dose escalation in HNSCC patients with persistent hypoxic sub-regions (9).

Questions remain over when and how imaging should be used to assist management of HNSCC patients with tumor hypoxia. Positron emission tomography (PET) data from patients with HNSCC have shown that high pre-treatment hypoxic volume indicate an increased risk of treatment failure (10). Furthermore – since imaging can monitor serial evolution of hypoxia during treatment – multiple independent PET studies have reported that persistence of hypoxic sub-volumes during chemoradiotherapy at 1-5 weeks may be most predictive of treatment failure (11-13) in patients with a variety of HNSCC subtypes, including HPV-associated OPC. Persistence of hypoxia following one week of chemoradiotherapy has been shown to occur in up to 50% of patients with HPV-associated OPC in studies using PET hypoxia imaging (7).

These data suggest that hypoxic volume may be a more useful clinical biomarker than hypoxic fraction, which is the favored biomarker used in preclinical studies (14), and may assist in future adaptive radiotherapy strategies. However, few studies have compared the hypoxia modification observed in both primary tumor and nodal metastases following treatment, or the timing of these changes (15). This is potentially important to determine optimum radiotherapy planning.

Oxygen-enhanced (OE)-MRI is a non-invasive hypoxia imaging technique, with spatial resolution comparable to PET, that can be performed on standard MRI systems (16). In the majority of OE-MRI studies, subjects inhale high-concentration oxygen (i.e. 100% O_2 gas) while T_1-weighted MRI is acquired. Well-oxygenated tissues exhibit increases in longitudinal relaxation rate (R_1) when breathing the hyperoxic gas whereas hypoxic regions have no significant change in R_1 (17). Changes in tissue R_1 (termed ΔR_1) and related OE-MRI biomarkers that measure MRI hypoxic fraction (HF_{MRI}) and hypoxic volume (HV_{MRI}) have identified and mapped hypoxia in animal models (18-21) and may predict outcome (22). The same OE-MRI biomarkers have detected hypoxia modification from chemoradiotherapy in animal models and in patients with lung cancer (23).

Previous work has shown that OE-MRI is feasible in patients with HNSCC (24). The primary purpose of this study was to determine if OE-MRI derived HV_{MRI} was repeatable in patients with HPV-associated OPC. The second purpose was to characterize the onset, duration, and within-patient variation of radiotherapy-induced changes in HV_{MRI} and other OE-MRI-derived biomarkers including ΔR_1 and HF_{MRI} as well as lesion whole tumor volume (WTV).

Methods

Patients with p16-positive OPC were recruited into a prospective clinical trial (ClinicalTrails.gov NCT03646747) with institutional review board approval (REC 18/NW/0563), in accordance with the Declaration of Helsinki. Patients provided written informed consent and were scanned at The Christie NHS Foundation Trust between March 2021 and January 2024.

Inclusion criteria were patients aged 18 or over with biopsy-proven OPC who were due to start definitive (chemo)radiotherapy with no metastatic disease outside of the local neck nodes. Biopsy samples showing strong, diffuse cytoplasmic and nuclear staining in >70% of tumor cells were classified as p16-positive, where p-16 immunohistochemistry represents a surrogate marker of previous HPV infection (25). Patients were also required to have ECOG performance status 0-2, creatinine clearance (Cockcroft-Gault) ≥30 mL/min, be able to lie comfortably for up to 60 minutes, no history of severe COPD, and be willing and able to consent to the study. Exclusion criteria were previous cancer therapy, pregnancy, history of gadolinium allergy or contraindication to MRI scanning.

MRI was performed on either a 1.5 T diagnostic MR (Philips Ingenia MR-RT, Philips Medical Systems, Best) or a 1.5 T MR Linac system (Elekta Unity, Elekta, Sweden), as both systems perform OE-MRI equivalently (24). Patients underwent MR imaging prior to radiotherapy (baseline 1, BL1), followed by scans at week 2 (W2) and/or week 4 (W4) into commencing radiation treatment. A subset of patients had two pre-treatment scans to enable repeatability assessment, baseline 0 and 1 (BL0 and BL1) at one week apart. All patients received radiotherapy prescriptions between 55 Gy in 20 fractions (#) to 70 Gy in 35#. Concurrent platinum-based therapy was given to eligible patients, following international practice.

MRI sequences were harmonised between the two MR systems (Supplementary Figure S1; Supplementary Table S1 for receive coil information and additional sequence parameter details). Patients were set up in the treatment position on a flat table top, without thermoplastic shell, on

both MR systems. Imaging was acquired in the transverse plane covering the neck region (11.2 cm craniocaudal coverage), and MR imaging sequences included:

1. T_2-weighted fast-spin echo (FSE) multi-slice anatomical imaging with Dixon-based fat suppression.
2. T_1 relaxation time measurement (3D inversion recovery turbo field echo (IRTFE), 3x3x5 mm^3, inversion pre-pulse delay times (TI) = 100, 500, 800, 1100, 4300 ms).
3. Dynamic OE-MR acquisition using the same 3D IRTFE sequence with TI = 1100 ms, 91 measurement time points, temporal resolution = 12 s. Gases were delivered at 15 L/min through a high-concentration, non-rebreathe oxygen mask (Ecolite^{TM}, Intersurgical Ltd). Initially medical air was given (dynamic time points 1-25, 5 mins) then 100% oxygen (dynamics 26-70, 9 mins), finally returning to medical air (dynamics 71-91, 4 mins).
4. DCE-MRI acquired using a 3D T_1-weighted fast field echo (FFE) Dixon sequence (3x3x5 mm^3) with IV contrast agent injection (Dotarem, 0.2 ml/kg (0.1 mmol/kg) at 3 ml/s with 20ml saline flush), delivered by contrast power injector (Experion, Bayer) at the 8th of 45 dynamic measurement time points.
5. Post-contrast 3D T_1-weighted FFE acquisition with spectral fat saturation to assist lesion delineation.

Image processing and analysis was carried out in MATLAB (R2018a, Mathworks, USA, RRID:SCR_001622). Motion correction and registration was carried out using Elastix (v5.0.1, https://elastix.lumc.nl) (26, 27). Primary tumors (T) and regional neck metastatic nodal (N) lesions were delineated on post-contrast T_1-weighted images by a HNC clinical oncologist (7 years' experience) using JIM software (JIM 6, Xinapse Systems, UK, RRID:SCR_009589). Lesion WTV was calculated in cm^3.

T_1 maps (units ms) obtained on air breathing (21% O_2) were derived by non-linear least squares fitting to the IRTFE signal (S(TI) acquired at the five TI values. This sequence employed TR > $5T_1$ and very short TE, such that the TR and TE terms can be ignored and the non-linear fit estimation of T_1 is:

$$S(TI) = S_0 \left| 1 - 2\lambda \exp\left(\frac{-TI}{T_1}\right) \right|, \quad \text{[equation 1]}$$

where, S_0 is the equilibrium signal, TI is the inversion pre-pulse delay time and λ is the inversion efficiency parameter. S_0, T_1 and λ were set as free parameters during fitting. Measurement of native T_1 permitted estimation of $R_1(t)$ (= $1/T_1(t)$ (units s^{-1}) during the dynamic OE-MRI acquisition as:

$$R_1(t) = -\frac{1}{TI} \ln \left\{ \frac{1 - \left[\frac{S(t)}{S_{air}} \left(1 - 2\lambda \exp\left(\frac{-TI}{T_1}\right) \right) \right]}{2\lambda} \right\}, \quad \text{[equation 2]}$$

where, S(t) is the raw signal intensity and S_{air} is the median of S(t) measurement time points 2-25, acquired during the air phase. Per-voxel change in R_1 was calculated by $\Delta R_1 = R_{1,O2} - R_{1,air}$ (28), with $R_{1,air}$ as the median of $R_1(t)$ measurement time points 2-25, acquired during the air phase and $R_{1,O2}$ as the median of $R_1(t)$ over time points 60-70, acquired at the end of the period of 100% oxygen inhalation. Lesion ΔR_1 was calculated as the median of voxel-wise ΔR_1 values per lesion.

Next, dynamic OE-MRI identified voxels where the signal intensity enhanced significantly ($p<0.05$) between air (time points 2-25) and 100% oxygen (time points 60-70) breathing phases using a paired t-test (29). Similarly, DCE-MRI data identified voxels where signal enhanced significantly ($p<0.05$) between pre- (time points 2-8) and post-contrast (time points 15-45) measurements. Voxels which enhanced on DCE-MRI but not on OE-MRI data were classed as hypoxic (19), enabling calculation of MRI hypoxic fraction (HF_{MRI}; unitless) and hypoxic volume (HV_{MRI}; units cm^3) (Supplementary Figure S2). Voxels that enhanced on both OE-MRI and DCE-MRI were classed as normoxic, allowing estimation of the normoxic volume (NV_{MRI}; cm^3). Voxels that did not enhance on DCE-MRI or OE-MRI were classed non-perfused (19). Quality control steps included checking for protocol adherence, acceptable native T_1 value, and absence of motion following motion correction.

No formal sample size calculation was performed in this exploratory study. OE-MRI derived parameters ΔR_1, $HF_{MRI,}$ HV_{MRI} NV_{MRI} as well as WTV were assessed for distribution normality using a Shapiro-Wilk test. The within-subject coefficient of variation (wCV) and repeatability coefficient (RC), with limits of agreement (LOA), were calculated, and where data were not normal, data underwent log-transformation (30). Back-transformed data provided asymmetric upper (RC_U) and lower (RC_L) LOA on RC.

Cohort change was assessed using mixed effects modelling to account for multiple lesions with patient clustering as a random effect; analysis was performed in STATA (BE 17.0, StataCorp, USA, RRID:SCR_012763) (31). Multiple comparisons between baseline and W2 and/or W4 were considered. In cases where patients had two baseline visits, the mean of the parameter values for the two baseline visits (BL0, BL1) was taken. Per-lesion level analysis was assessed if change in parameter values from baseline exceeded the calculated RC LOA, and in doing so were considered as real change (30). $P < 0.05$ was considered significant in all statistical assessments.

Data Availability

Data were generated by the authors and available on request, since an appropriate recognized platform for sharing the study data does not exist.

Results

OE-MRI is well-tolerated in patients with oropharyngeal carcinoma

In total, 27 patients with confirmed p16-positive OPC were recruited, as summarised in Supplementary Figure S3. Data were not included from three patients (one patient had no measurable disease on MRI, one had data acquired with protocol deviations at baseline and one patient had gas inhalation failure at baseline). Therefore, 24 patients (median age, 67 years [59 – 75 interquartile range], 21 males) were included in the main study for subsequent analysis.

The number of days (mean (± standard deviation) between double baseline imaging sessions was 6 (± 2) days. There were 12 (± 4) days from radiotherapy start to W2 imaging and 30 (± 8) days between radiotherapy start to W4 imaging.

Motion correction was successful in all but four lesion datasets which could not be corrected (patients 11 (tumor) & 20 (tumor) one of two baseline scans, patient 13 W4 (tumor and node) scan). Example motion corrected ΔR_1 time-courses are shown in Supplementary Figure S4A-C. Additionally, contrast agent delivery was not successful in patient 31 at W2 and so data at this time point is also not included. The primary tumor of patient 37 had responded to become non-measurable by W4 due to excellent clinical response and so it was only possible to include nodal data at this time point for this patient. Additional imaging visits are absent at W2 and W4 relating to four patients unable to attend due to COVID19 infection and isolation or department closure during the pandemic and other patients being unable to attend imaging as they became too unwell, during standard of care treatment.

Details of patient demographics, tumor site, stage, treatment regimen, target lesions imaged and imaging timepoints (i.e. BL0, BL1, W2 and W4) which had useable data are provided in Table 1. The scan session lasted 50-60 minutes, including patient setup. No patient adverse events were reported.

Baseline WTV are listed for all lesions in Supplementary Table S2. Of the 24 patients (44 lesions), included in the main study, baseline (BL) HV_{MRI} ranged from 1.3 to 82.1 cm^3 with a median [interquartile range (IQR)] HV_{MRI} of 10.3 cm^3 [5.7, 24.6]).

OE-MRI biomarkers are repeatable

Repeatability assessment was performed in 12 patients (21 lesions; 11T, 10N) (Supplementary Figure S5A-E) who attended BL0 and BL1 imaging sessions. None of the imaging biomarkers were normally distributed and so all underwent log transformation (parameter histograms and Shapiro-Wilk test results provided in Supplementary Figure S6A-E and Supplementary Table S3 respectively). The median [IQR] of the HV_{MRI} values at the two baseline time points were 16.0 cm^3 [6.4, 36.0] and 10.5 cm^3 [6.6, 43.6]. The HV_{MRI} wCV was 24.6% and the RC limits of agreement (LOA) were RC_L = -45.7% and RC_U = 84.1%.

Repeatability information for other imaging biomarkers is listed for comparison in Table 2. Non-perfused volumes of tumor were negligible for all except two patients and are not included further in the analyses.

HV_{MRI} detects hypoxia modification following therapy across the cohort

Biological response to therapy – here hypoxia modification – was examined in the cohort by assessing the change in HV_{MRI} from pre-treatment baseline (BL) to W2 and W4. BL was defined as either BL1, for those with one baseline visit, or as the mean of baseline measurements, for those with two baseline visits (i.e. BL0 and BL1). In all, 20 patients (36 lesions: 19 primary tumors, 17 nodal lesions), with a BL scan and at least a W2 or W4 scan or both, were evaluated.

Example ΔR_1 data (Supplementary Figure S7A-C) and hypoxia maps are provided (Figure 1A) for the nodal tumor in patient 7. In this example, HV_{MRI} shows reduction beyond the RC LOA threshold during treatment (i.e. reduction beyond RC_L = –45.7% from BL). Comparative lack of change results for NV_{MRI} and non-perfused tissue are shown (Figure 1B).

At W2, 18 patients (33 lesions: 17 primary tumors, 16 nodal lesions) had imaging. A cohort-level reduction in HV_{MRI} was observed, with median baseline hypoxic volume of 11.3 cm^3 [6.8, 28.3] that reduced at W2 to 6.9 cm^3 [3.5, 13.0] ($p < 0.001$) (Supplementary Table S4). At W4, imaging was only obtained in 12 patients, but a significant cohort-level reduction in HV_{MRI} was detected (20 lesions: 10 primary tumors, 10 nodal lesions) from baseline down to 5.9 cm^3 [2.4, 8.6] ($p < 0.001$). The corresponding mean (± standard error) values of HV_{MRI} are 20.2 (± 3.5) cm^3 (BL), 10.3 (± 1.7) cm^3 (W2) and 6.5 (± 1.2) cm^3 (W4).

For comparison, a significant increase in ΔR_1 and decrease in HF_{MRI} were observed at W2 and W4 ($p \leq 0.001$) (Supplementary Table S4). In distinction, the NV_{MRI} did not change at W2, whereas the overall WTV was reduced ($p < 0.001$). Cohort changes for all imaging biomarkers are displayed as plots of the standard error on the mean (SEM) in Figure 1C and change in individual lesions are also provided (Supplementary Figure S8A-E).

HV_{MRI} identifies the incidence and onset of hypoxia modification

The change in HV_{MRI} was calculated for each lesion. This was compared to the RC LOA, ($\%RC_L$, $\%RC_U$ = -45.7%, 84.1%) (see Table 2) to determine if HV_{MRI} increased or decreased in an individual lesion more than could be expected by chance (30).

Hypoxia modification was identified. Data were assessed in 18 patients (with 33 lesions) at W2 and in 12 patients (20 lesions) at W4. At W2, 18/33 (54.5%) of all lesions had a significant reduction in HV_{MRI}. Overall, 10/17 (58.8%) primary tumors and 8/16 (50.0%) nodal lesions had lesion-specific reduction in HV_{MRI} (Figure 2A). At W4, there was even greater evidence of hypoxia change, with a significant reduction in HV_{MRI} in 15/17 (88.2%) of all lesions, comprising 6/8 (75.0%) primary tumors and 9/9 (100%) nodal lesions. In all, 36 lesions were evaluated at W2 and/or W4. Of these, 26/36 (72.2%) showed reduction in HV_{MRI} by their last scan.

The persistence of hypoxia modification was examined in 10 patients (comprising 17 lesions) who had scans at both W2 and W4. Of these, 2/17 (11.8%) lesions had no reduction in HV_{MRI} at W2 or

W4; 5/17 (29.4%) lesions had reduction in HV_{MRI} that was only significant by W4; 10/17 (58.8%) lesions had reduction in HV_{MRI} by W2, all of which showed persistent hypoxia modification at W4 (Figure 2B).

HV_{MRI} characterizes concordance in hypoxia modification in primary and nodal tumors

Change in HV_{MRI} were examined at W2 or W4 for the 14 patients who had both primary and nodal lesions. Presence or absence of HV_{MRI} change beyond the RC LOA was limits were recorded. Fully concordant change – where both primary and nodal lesions behaved in the same manner at all available image timepoints – was seen in 7/14 (50.0%) patients.

Notably, fully discordant changes occurred in 6/14 patients (42.9%) which was marked in four patients (Table 3). This included examples both of primary tumors having hypoxia modification while nodal tumors remained unchanged (patients 7 and 20) and, conversely, of primary tumors remaining unchanged while nodal tumors showed hypoxia modification (patients 9 and 37). In two of the cases, discordant changes were more marginal (patients 12 and 18). Finally, one patient (patient 29) had initial discordant change in their primary and nodal lesions at W2, followed by concordant change (reduction in HV_{MRI}) at W4.

HV_{MRI} and WTV reduction have multiple distinct patterns

The change in HV_{MRI} at W2 was compared to changes in normoxic volume (NV_{MRI}) and WTV. At W2, the 18/33 lesions with hypoxia modification had two distinct patterns of change. Eleven lesions had significant reduction in NV_{MRI} and therefore had associated reduction in overall WTV (Figure 3A). In distinction, seven lesions had no significant change in WTV despite reduction in HV_{MRI} because the NV_{MRI} did not reduce significantly and in some cases increased beyond the RC LOA (Figure 3B).

The remaining 15/33 lesions had no hypoxia modification at W2 (i.e. HV_{MRI} did not reduce beyond the RC LOA). Of these, four lesions had significant reduction in WTV despite lack of hypoxia modification, driven by significant reduction in NV_{MRI} (Figure 3C). Eleven lesions had no reduction in WTV relating to no significant reduction in either HV_{MRI} or NV_{MRI} (indeed, one lesion had significant increase in WTV, driven by increase in the NV_{MRI}) (Figure 3D).

We also compared the hypoxia change induced by therapy by measuring hypoxic fraction (HF_{MRI}) as well as HV_{MRI}. Changes in HF_{MRI} mirrored changes in HV_{MRI} except for 6 lesions where the HF_{MRI} did not change despite reduction in HV_{MRI}. In these 6 lesions, the WTV, HV_{MRI} and NV_{MRI} all reduced in similar proportions, thereby not affecting the proportion of hypoxic to normoxic tissue and rendering HF_{MRI} insensitive to radiation-induced treatment effects.

Discussion and Conclusion

Hypoxia is a major driver of resistance to therapy in HNSCC patients including those with HPV-associated OPC (2). Data from hypoxia PET, the most common modality used to image hypoxia (32) suggests that persistent low tumor oxygenation during early treatment with radiotherapy predicts treatment failure (11, 12). Prospective trials of adaptive radiotherapy based on early change in PET hypoxia status, for example when identified from FMISO-PET imaging, suggest a potential strategy to personalize dose delivery and improve disease control while reducing unnecessary radiotherapy-related side-effects (9, 33). In particular, recent data from the 30 ROC trial suggest that hypoxia measurement is important for the management of dose de-escalation strategies (8).

Sparse hypoxia tracer availability, high cost and limited infrastructure capable of performing PET hypoxia imaging have hindered widespread clinical adoption. OE-MRI is an affordable and practical alternative to PET for the assessment of radiation-induced hypoxia modification in patients with NSCLC (23). Here, we sought to determine if OE-MRI HV_{MRI} was repeatable in patients with newly diagnosed p16-positive OPC. We then aimed to evaluate the incidence, onset and variation in hypoxia modification induced by (chemo)radiotherapy.

Our data provide evidence that OE-MRI, when combined with perfusion imaging, is feasible, tolerable and can detect cohort changes in hypoxia, thus offering an alternative to hypoxia PET imaging in patients with HNSCC. Oxygen-enhancement in tissues was measured by ΔR_1 which indicated technique success in all patients, consistent with an independent study (34) but contrary to findings in HNSCC from a different laboratory (35). ΔR_1 increase observed in our patient population is consistent with tissue re-oxygenation (36) following fractionated radiotherapy. Median values and ranges of ΔR_1, HV_{MRI} and HF_{MRI} were defined. Cohort level reductions were similar to those reported with OE-MRI HV_{MRI} in NSCLC (23) and in hypoxic volume using FMISO-PET (11, 12).

A key feature of this study was our examination of measurement precision. OE-MRI derived hypoxic volume (HV_{MRI}) showed good repeatability with a wCV of 24.6%, comparable with previous data in NSCLC (where HV_{MRI} wCV = 25.9%) (23). Other OE-MRI parameters and measures of WTV also showed good repeatability that are comparable with other quantitative imaging biomarkers such as K^{trans} (37-39). The RC LOA determined if and when therapy-induced changes in the HV_{MRI} of individual lesions could be considered real at a 95% confidence level (26). Identifying those lesions which experienced significant changes in hypoxia and those which did not, then enabled **three key findings** to be noted, each with translational implications.

Firstly, we identified the variable onset of hypoxia modification in individual lesions. We showed that 54.5% of all lesions had reduced HV_{MRI} at W2, with similar proportions of primary tumors and nodal metastases changing. The proportion of lesions exhibiting hypoxia reduction increased to nearly 90% at W4, with the caveat that fewer lesions were examined at that timepoint. Notably, all lesions with hypoxia reduction by W2 had persistent change to W4 and of equal note, some lesions with significant hypoxia modification only manifested this change by W4. This information provides insight beyond that derived from cohort analysis alone (40) and implies that dose de-escalation may be performed in around half of patients within 2 weeks of radiation-based therapy to achieve maximal benefit. In addition, more moderate dose de-escalation could be of benefit to another group of patients who show detectable hypoxia modification between weeks 2 to 4 of radiotherapy, although larger studies will need to determine the optimum patient benefit and cost-effectiveness.

Secondly, we examined patients with both primary tumors and nodal metastases. It is known that patients can have varying levels of hypoxia in their primary and nodal HNSCC tumors (15). However, the relative indicence of concordance and discordance of lesion hypoxia between primary and nodal tumors is not well understood. We identified that only half of patients had concordant hypoxia modification in both lesions, and that primary tumor and nodal metastases behaved differently, in the other half of patients (lesion changes were discordant). This implies that sampling only a single lesion through imaging or biopsy may provide an inaccurate picture of the

change in hypoxic status in a substantial proportion of clinical cases. Clinical decisions – such as whether to dose de-escalate or not – require an assessment of all locoregional lesions rather than one index lesion and may require individual dosing to specific nodal levels. It is even possible that future strategies may allow de-escalated treatment in nodes that demonstrate biological response while maintaining dose in others that do not have hypoxia modification. Such approaches become possible in the era of functional imaging assessment performed at regular on-therapy intervals on systems such as an MR Linac (41).

Thirdly, we showed that hypoxic volumes reduced significantly in over 20% of lesions that did not demonstrate overall size reduction in the early response to therapy. This implies that a number of patients have biological changes in their lesions that are not detected through conventional assessment of tumor size. Further work in larger patient numbers is needed to assess the relative importance of hypoxia modification as an additional covariate in predicting clinical outcome. In addition, we highlight the potential limitations of solely measuring hypoxic fraction (HF_{MRI}) as this measure can appear insensitive to treatment effects when both the hypoxic sub-volume and the overall tumor volume are reduced in an approximately equivalent ratio (42).

Some study limitations existed. While this study is the largest clinical OE-MRI study performed to date, several patients had missing data due to factors including scan cancellations during the COVID19 pandemic. It should also be noted that, in line with the general HNSCC population, patients recruited to this study were p16-positive which is considered an accepted method of identifying HPV-associated disease and these patients are known to respond superiorly to those with p16-negative HNSCC (43). Further work should assess whether similar OE-MRI data are obtained in patients with p16-negative disease.

Future studies are required to extend biological validation already obtained from multiple animal models (18-21), with hypoxia gene signatures and other methods in appropriate HNSCC clinical population. In addition, establishment of multicenter reproducibility in larger numbers of patients, across multiple vendor platforms and field strength will provide a more definitive estimate of RC

LOA for use in further clinical studies. Refinement of estimates of HV_{MRI} may also be required to distinguish acute transient hypoxia from established chronic hypoxia, the former of which may contribute to part of the variation in biomarker estimates between the two baseline scans.

Collectively, the data reported here add to our previous work in NSCLC and HNSCC (23, 24) to support the use of OE-MRI as a biological response assay. The technique can identify the onset, persistence, and variation in hypoxia modification in different lesions and different patients, making a strong case for the value of imaging assessment in studies that evaluate tumor hypoxia.

Acknowledgements

Michael Dubec acknowledges PhD funding support from the Medical Research Council (MRC). Michael Dubec, Damien McHugh, Ananya Choudhury, Marcel van Herk and James O'Connor are supported by Cancer Research UK Manchester Centre award [CTRQQR-2021\100010]. James O'Connor is supported by Cancer Research UK NCITA grant (C19221/A28683). Nuria Porta is supported by core programme grant from Cancer Research UK (C1491/A25351). James O'Connor is supported by Clinician Scientist Fellowship from Cancer Research UK (C19221/A15267). Marcel van Herk, Ananya Choudhury and James O'Connor are supported by National Institute for Health Research (NIHR) Manchester Biomedical Research Centre. Kevin Harrington and James O'Connor are supported by the National Institute for Health Research (NIHR) Biomedical Research Centre at The Royal Marsden NHS Foundation Trust and the Institute of Cancer Research, London. Kevin Harrington acknowledges support for the ICR/RM CRUK RadNet Centre of Excellence.

References

1. Harris AL. Hypoxia--a key regulatory factor in tumour growth. Nat Rev Cancer. 2002;2(1):38-47.

2. Overgaard J. Hypoxic radiosensitization: adored and ignored. J Clin Oncol. 2007;25(26):4066-74.

3. Minassian LM, Cotechini T, Huitema E, Graham CH. Hypoxia-Induced Resistance to Chemotherapy in Cancer. Adv Exp Med Biol. 2019;1136:123-39.

4. Dewhirst MW, Mowery YM, Mitchell JB, Cherukuri MK, Secomb TW. Rationale for hypoxia assessment and amelioration for precision therapy and immunotherapy studies. J Clin Invest. 2019;129(2):489-91.

5. Horsman MR, Mortensen LS, Petersen JB, Busk M, Overgaard J. Imaging hypoxia to improve radiotherapy outcome. Nat Rev Clin Oncol. 2012;9(12):674-87.

6. Chundury A, Kim S. Radiation Dose De-Escalation in HPV-Positive Oropharynx Cancer: When Will It Be an Acceptable Standard of Care? J Clin Oncol. 2021;39(9):947-9.

7. Lee N, Schoder H, Beattie B, Lanning R, Riaz N, McBride S, et al. Strategy of Using Intratreatment Hypoxia Imaging to Selectively and Safely Guide Radiation Dose De-escalation Concurrent With Chemotherapy for Locoregionally Advanced Human Papillomavirus-Related Oropharyngeal Carcinoma. Int J Radiat Oncol Biol Phys. 2016;96(1):9-17.

8. Lee NY, Sherman EJ, Schöder H, Wray R, Boyle JO, Singh B, et al. Hypoxia-Directed Treatment of Human Papillomavirus-Related Oropharyngeal Carcinoma. J Clin Oncol. 2024:JCO2301308:940-950.

9. Welz S, Paulsen F, Pfannenberg C, Reimold M, Reischl G, Nikolaou K, et al. Dose escalation to hypoxic subvolumes in head and neck cancer: A randomized phase II study using dynamic [18F]FMISO PET/CT. Radiother Oncol. 2022;171:30-6.

10. Saksø M, Mortensen LS, Primdahl H, Johansen J, Kallehauge J, Hansen CR, et al. Influence of FAZA PET hypoxia and HPV-status for the outcome of head and neck squamous cell carcinoma (HNSCC) treated with radiotherapy: Long-term results from the DAHANCA 24 trial (NCT01017224). Radiother Oncol. 2020;151:126-33.

11. Zips D, Zöphel K, Abolmaali N, Perrin R, Abramyuk A, Haase R, et al. Exploratory prospective trial of hypoxia-specific PET imaging during radiochemotherapy in patients with locally advanced head-and-neck cancer. Radiother Oncol. 2012;105(1):21-8.

12. Wiedenmann NE, Bucher S, Hentschel M, Mix M, Vach W, Bittner MI, et al. Serial [18F]-fluoromisonidazole PET during radiochemotherapy for locally advanced head and neck cancer and its correlation with outcome. Radiother Oncol. 2015;117(1):113-7.

13. Löck S, Perrin R, Seidlitz A, Bandurska-Luque A, Zschaeck S, Zöphel K, et al. Residual tumour hypoxia in head-and-neck cancer patients undergoing primary radiochemotherapy, final results of a prospective trial on repeat FMISO-PET imaging. Radiother Oncol. 2017;124(3):533-40.

14. Singleton DC, Macann A, Wilson WR. Therapeutic targeting of the hypoxic tumour microenvironment. Nat Rev Clin Oncol. 2021;18(12):751-72.

15. Bandurska-Luque A, Löck S, Haase R, Richter C, Zöphel K, Perrin R, et al. Correlation between FMISO-PET based hypoxia in the primary tumour and in lymph node metastases in locally advanced HNSCC patients. Clin Transl Radiat Oncol. 2019;15:108-12.

16. Dewhirst MW, Birer SR. Oxygen-Enhanced MRI Is a Major Advance in Tumor Hypoxia Imaging. Cancer Res. 2016;76(4):769-72.

17. O'Connor JPB, Robinson SP, Waterton JC. Imaging tumour hypoxia with oxygen-enhanced MRI and BOLD MRI. Br J Radiol. 2019;92(1095):20180642.

18. Colliez F, Neveu MA, Magat J, Cao Pham TT, Gallez B, Jordan BF. Qualification of a noninvasive magnetic resonance imaging biomarker to assess tumor oxygenation. Clin Cancer Res. 2014;20(21):5403-11.

19. O'Connor JP, Boult JK, Jamin Y, Babur M, Finegan KG, Williams KJ, et al. Oxygen-Enhanced MRI Accurately Identifies, Quantifies, and Maps Tumor Hypoxia in Preclinical Cancer Models. Cancer Res. 2016;76(4):787-95.

20. White DA, Zhang Z, Li L, Gerberich J, Stojadinovic S, Peschke P, et al. Developing oxygen-enhanced magnetic resonance imaging as a prognostic biomarker of radiation response. Cancer Lett. 2016;380(1):69-77.

21. Linnik IV, Scott ML, Holliday KF, Woodhouse N, Waterton JC, O'Connor JP, et al. Noninvasive tumor hypoxia measurement using magnetic resonance imaging in murine U87 glioma xenografts and in patients with glioblastoma. Magn Reson Med. 2014;71(5):1854-62.

22. Arai TJ, Yang DM, Campbell JW, Chiu T, Cheng X, Stojadinovic S, et al. Oxygen-Sensitive MRI: A Predictive Imaging Biomarker for Tumor Radiation Response? Int J Radiat Oncol Biol Phys. 2021;110(5):1519-29.

23. Salem A, Little RA, Latif A, Featherstone AK, Babur M, Peset I, et al. Oxygen-enhanced MRI Is Feasible, Repeatable, and Detects Radiotherapy-induced Change in Hypoxia in Xenograft Models and in Patients with Non-small Cell Lung Cancer. Clin Cancer Res. 2019;25(13):3818-29.

24. Dubec MJ, Buckley DL, Berks M, Clough A, Gaffney J, Datta A, et al. First-in-human technique translation of oxygen-enhanced MRI to an MR Linac system in patients with head and neck cancer. Radiother Oncol. 2023;183:109592.

25. Price JM, West CM, Mistry HB, Betts G, Bishop P, Kennedy J, et al. Improved survival prediction for oropharyngeal cancer beyond TNMv8. Oral Oncol. 2021;115:105140.

26. Klein S, Staring M, Murphy K, Viergever MA, Pluim JP. elastix: a toolbox for intensity-based medical image registration. IEEE Trans Med Imaging. 2010;29(1):196-205.

27. Shamonin DP, Bron EE, Lelieveldt BP, Smits M, Klein S, Staring M, et al. Fast parallel image registration on CPU and GPU for diagnostic classification of Alzheimer's disease. Front Neuroinform. 2013;7:50.

28. Huen I, Morris DM, Wright C, Parker GJ, Sibley CP, Johnstone ED, et al. R1 and R2 * changes in the human placenta in response to maternal oxygen challenge. Magn Reson Med. 2013;70(5):1427-33.

29. Little RA, Jamin Y, Boult JKR, Naish JH, Watson Y, Cheung S, et al. Mapping Hypoxia in Renal Carcinoma with Oxygen-enhanced MRI: Comparison with Intrinsic Susceptibility MRI and Pathology. Radiology. 2018;288(3):739-47.

30. Obuchowski NA. Interpreting Change in Quantitative Imaging Biomarkers. Acad Radiol. 2018;25(3):372-9.

31. Gelman A, Hill J. Data analysis using regression and multilevel/hierarchical models: Cambridge university press; 2006.

32. Tatum JL, Kelloff GJ, Gillies RJ, Arbeit JM, Brown JM, Chao KS, et al. Hypoxia: importance in tumor biology, noninvasive measurement by imaging, and value of its measurement in the management of cancer therapy. Int J Radiat Biol. 2006;82(10):699-757.

33. Riaz N, Sherman E, Pei X, Schöder H, Grkovski M, Paudyal R, et al. Precision Radiotherapy: Reduction in Radiation for Oropharyngeal Cancer in the 30 ROC Trial. J Natl Cancer Inst. 2021;113(6):742-51.

34. McCabe A, Martin S, Rowe S, Shah J, Morgan PS, Borys D, et al. Oxygen-enhanced MRI assessment of tumour hypoxia in head and neck cancer is feasible and well tolerated in the clinical setting. Eur Radiol Exp. 2024;8(1):27.

35. Bluemke E, Bertrand A, Chu KY, Syed N, Murchison AG, Cooke R, et al. Oxygen-enhanced MRI and radiotherapy in patients with oropharyngeal squamous cell carcinoma. Clin Transl Radiat Oncol. 2023;39:100563.

36. Telarovic I, Wenger RH, Pruschy M. Interfering with Tumor Hypoxia for Radiotherapy Optimization. J Exp Clin Cancer Res. 2021;40(1):197.

37. O'Connor JP, Carano RA, Clamp AR, Ross J, Ho CC, Jackson A, et al. Quantifying antivascular effects of monoclonal antibodies to vascular endothelial growth factor: insights from imaging. Clin Cancer Res. 2009;15(21):6674-82.

38. Peled S, Vangel M, Kikinis R, Tempany CM, Fennessy FM, Fedorov A. Selection of Fitting Model and Arterial Input Function for Repeatability in Dynamic Contrast-Enhanced Prostate MRI. Acad Radiol. 2019;26(9):e241-e51.

39. Jayson GC, Zhou C, Backen A, Horsley L, Marti-Marti K, Shaw D, et al. Plasma Tie2 is a tumor vascular response biomarker for VEGF inhibitors in metastatic colorectal cancer. Nat Commun. 2018;9(1):4672.

40. O'Connor JP, Jackson A, Asselin MC, Buckley DL, Parker GJ, Jayson GC. Quantitative imaging biomarkers in the clinical development of targeted therapeutics: current and future perspectives. Lancet Oncol. 2008;9(8):766-76.

41. Datta A, Aznar MC, Dubec M, Parker GJM, O'Connor JPB. Delivering Functional Imaging on the MRI-Linac: Current Challenges and Potential Solutions. Clin Oncol (R Coll Radiol). 2018;30(11):702-10.

42. Lehtiö K, Eskola O, Viljanen T, Oikonen V, Grönroos T, Sillanmäki L, et al. Imaging perfusion and hypoxia with PET to predict radiotherapy response in head-and-neck cancer. Int J Radiat Oncol Biol Phys. 2004;59(4):971-82.

43. Lassen P, Eriksen JG, Hamilton-Dutoit S, Tramm T, Alsner J, Overgaard J, et al. HPV-associated p16-expression and response to hypoxic modification of radiotherapy in head and neck cancer. Radiother Oncol. 2010;94(1):30-5.

Figure legends

Figure 1. Treatment-induced changes in OE-MRI derived biomarkers. (A) Example hypoxia maps for a large metastatic lymph node (Patient 7) obtained at two baseline timepoints (BL0, BL1) and weeks 2 (W4) and 4 (W4) of radiation treatment. Corresponding ΔR_1 maps are provided in Supplementary Figure S7A-C. (B) Bar charts plot the relative sizes of HV_{MRI} along with NV_{MRI} and non-perfused volume for this patient. Note – the combination of HV_{MRI}, NV_{MRI} and non-perfused volume equate to the WTV. (C) Patient cohort assessment of treatment effects illustrated as plots of standard error on the mean (SEM) for (top left to bottom right) HV_{MRI}, NV_{MRI}, non-perfused volume, WTV, HF_{MRI} and ΔR_1.

***Figure 2**. Hypoxic volume (HV_{MRI}) changes at week 2 (W2). (A) Waterfall plot showing the percentage change in HV_{MRI} from baseline to W2 in all lesions, categorized as primary tumors or nodal metastases. (B) Analysis of the 17 lesions imaged at both W2 and W4 compares the reduction from baseline at W2 (light blue) and W4 (dark blue). Dashed lines are the asymmetrical RC LOA for HV_{MRI} (i.e. -45.7% and +84.1%).*

***Figure 3**: Waterfall plots showing change in HV_{MRI}, NV_{MRI} and WTV at week 2 (W2). Four patterns seen were (A) lesions with significant hypoxia modification as well as reduction in WTV. Diamonds indicate tumors where the hypoxic fraction remained unchanged; (B) tumors with significant hypoxia modification that did not have change in WTV; (C) tumors that did not have significant individual changes in hypoxia, but significant reduction in WTV was driven by reduction in NV_{MRI}; (D) tumors with no reduction in HV_{MRI}, NV_{MRI} or WTV.*

Figure 1

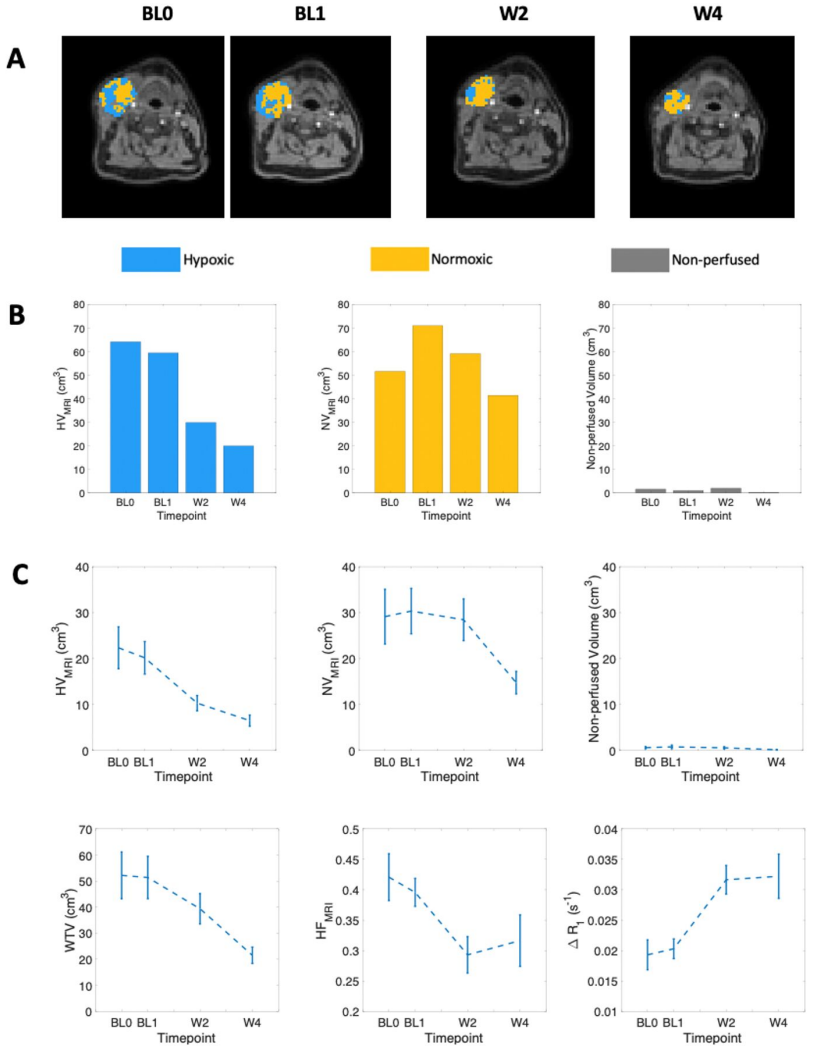
A
BL0
BL1
W2
W4
Hypoxic
Normoxic
Non-perfused
B
HV_{MRI} (cm^3)
NV_{MRI} (cm^3)
Non-perfused Volume (cm^3)
Timepoint
C
WTV (cm^3)
HF_{MRI}
ΔR_1 (s^{-1})

Figure 2

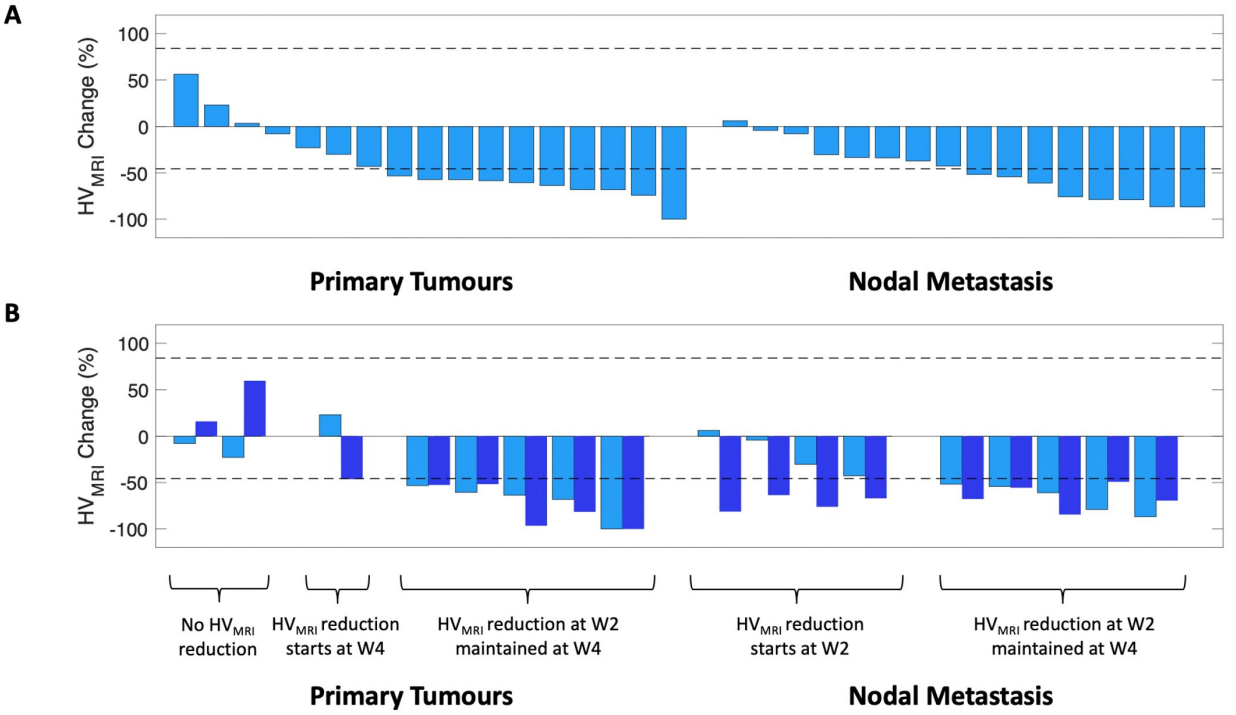
A
100
50
0
-50
-100
HVMRI Change (%)
Primary Tumours
Nodal Metastasis
B
100
50
0
-50
-100
HVMRI Change (%)
No HVMRI reduction
HVMRI reduction starts at W4
HVMRI reduction at W2 maintained at W4
HVMRI reduction starts at W2
HVMRI reduction at W2 maintained at W4
Primary Tumours
Nodal Metastasis

Figure 3

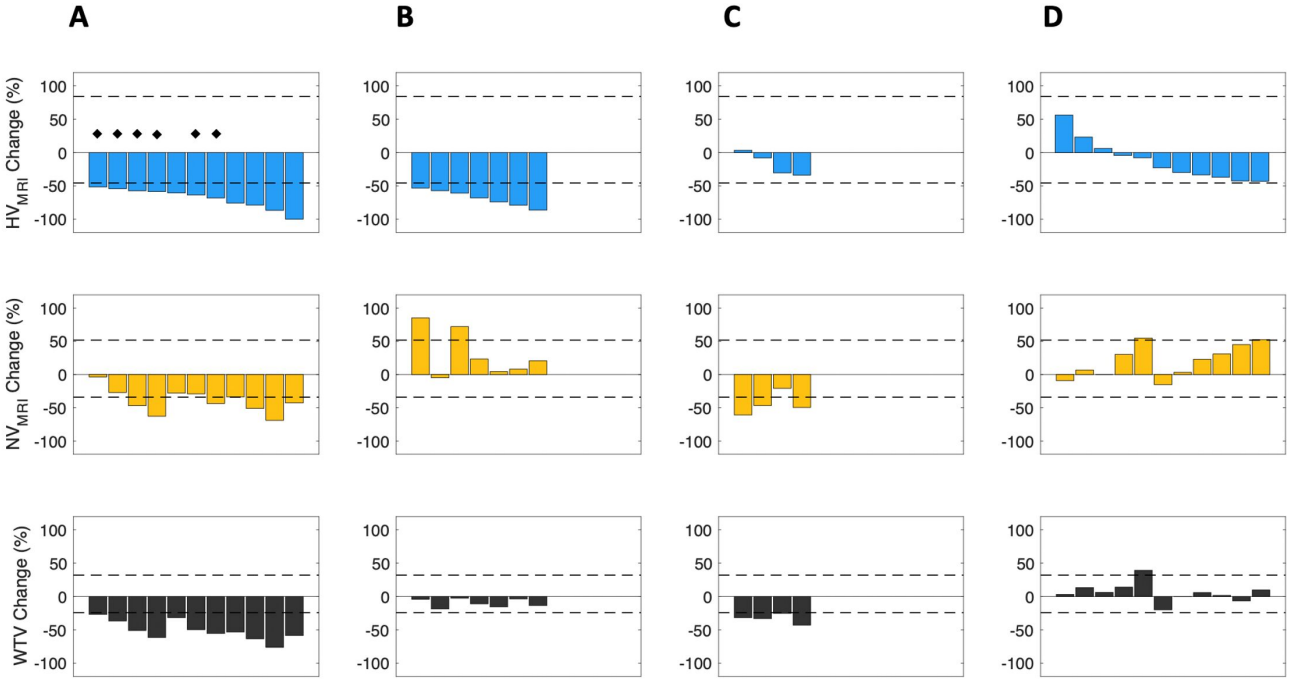

ID	Sex	Age	Disease Sub-site	TNMv8 Stage	Treatment (dose(Gy)/fractions, (chemotherapy)	Target Lesion	Imaging Acquired				MR System
							BL0	BL1	W2	W4	
2	F	74	Tonsil	T3 N1	55/20	T	✔	✔	✔		Diagnostic MR
3	F	56	Tonsil	T4 N0	70/35 and cisplatin (weekly)	T		✔	✔		Diagnostic MR
4	M	72	Tonsil	T2 N1	55/20	T, N	✔	✔	✔	✔	Diagnostic MR
7	M	64	Tonsil	T3 N1	66/30 and carboplatin (weekly)	T, N	✔	✔	✔	✔	Diagnostic MR
9	M	76	Tonsil	T3 N2	55/20	T, N, N		✔	✔		Diagnostic MR
10	M	79	Tonsil	T2 N1	55/20	T, N		✔			Diagnostic MR
11	F	61	Tonsil	T4 N0	66/30 and cisplatin (3-weekly)	T	*	✔	✔		Diagnostic MR
12	M	58	Tonsil	T3 N1	66/30 and cisplatin (3-weekly)	T, N, N	✔	✔	✔		Diagnostic MR
13	M	71	Tonsil	T4 N1	70/35 and cisplatin (weekly)	T, N		✔	✔	*	Diagnostic MR
14	M	65	Soft palate	T2 N0	66/30	T	✔	✔		✔	MR Linac
16	M	66	Tongue base	T1 N3	66/30 and cisplatin (3-weekly)	T	✔	✔	✔	✔	MR Linac
18	M	60	Tonsil	T3 N1	66/30 and cisplatin (3-weekly)	T, N	✔	✔	✔		MR Linac
19	M	77	Tongue base	T4 N2	66/30	T, N		✔	✔	✔	Diagnostic MR
20	M	67	Tongue base	T2 N2	66/30 and cisplatin (3-weekly)	T, N	✔*	✔	✔	✔	Diagnostic MR
21	M	74	Tongue base	T4 N1	66/30	T, N	✔	✔	✔	✔	Diagnostic MR
22	M	67	Tongue base	T2 N3	66/30 and carboplatin (3-weekly)	T, N		✔			Diagnostic MR
23	M	77	Tongue base	T1 N1	55/20	T, N	✔	✔	✔		MR Linac
24	M	53	Tonsil	T4 N1	55/20	T, N		✔			Diagnostic MR
28	M	57	Tonsil	T4 N1	66/30 and cisplatin (3-weekly)	N		✔	✔	✔	Diagnostic MR
29	M	75	Tonsil	T4 N1	55/20	T, N		✔	✔	✔	MR Linac
30	M	75	Tongue base	T1 N1	66/30	N, N		✔			Diagnostic MR
31	M	53	Tonsil	T2 N1	66/30 and cisplatin (3-weekly)	T, N		✔	‡	✔	MR Linac
35	M	63	Tonsil	T3 N1	66/30 and cisplatin (3-weekly)	T, N	✔	✔	✔	✔	MR Linac
37	M	51	Tongue base	T2 N1	66/30 and cisplatin (3-weekly)	T, N	✔	✔	✔	✔§	MR Linac

Table 1*. Clinical information and MRI scan details for image datasets from the 24 patients used in subsequent analysis. Target lesions imaged, T = Primary tumor, N = local metastatic lymph node. BL0, BL1, W2 and W4 refer to baseline 0 and 1 and week 2 and 4 of treatment, respectively. *Datasets not included in analysis due to motion corruption included patient 11, tumor baseline, patient 13 tumor and node at W4, and patient 20 tumor at baseline. ‡Contrast agent delivery was not carried out on patient 31 at W2 and so data at this time point is not included. §Patient 37 tumor was non-measurable at W4 and not included.*

Parameter	BL0 (Median [IQR])	BL1 (Median [IQR])	wCV (95% CI)	RC LOA (RC_L, RC_U)
ΔR_1 (s^{-1})	0.017 [0.011, 0.026]	0.018 [0.013, 0.025]	31.5% (23.5 – 48.0%)	-53.2%, 113.8%
HF_{MRI}	0.46 [0.30, 0.53]	0.45 [0.29, 0.54]	20.4% (15.3 – 30.4%)	-40.2%, 67.2%
HV_{MRI} (cm^3)	16.0 [6.4, 36.0]	10.5 [6.6, 43.6]	24.6% (18.5 – 37.0%)	-45.7%, 84.1%
NV_{MRI} (cm^3)	21.3 [9.2, 41.9]	20.6 [10.6, 46.2]	16.3% (12.3 – 24.0%)	-34.1%, 51.8%
WTV (cm^3)	37.7 [17.6, 76.7]	35.0 [20.0, 87.2]	10.6% (8.0 – 15.4%)	-24.3%, 32.1%

***Table 2**. Pre-treatment repeatability data for 21 lesions from 12 patients acquired at two pre-treatment baseline timepoints (B0 and B1). IQR = inter-quartile range, wCV = within-subject coefficient of variation, 95% CI = 95% confidence intervals on wCV, RC = repeatability coefficient, LOA = limits of agreement, RC_L = RC lower limit of agreement, RC_U = RC upper limit of agreement.*

Patient ID	Lesion	HV_{MRI} W2	HV_{MRI} W4	Concordant change between lesions?	Comments
4	T	↓	↓	Yes	
	N	↓	↓		
7	T	NC	NC	No	N had reduced HV_{MRI} at both W2 and W4, but T did not
	N	↓	↓		
9	T	↓		No	T had reduced HV_{MRI} at W2, but N1 and N2 did not
	N1	NC			
	N2	NC			
12	T	↓		No (but equivocal)	T and N2 reduced HV_{MRI} at W2 N1 hypoxia decrease of 37.1% approached the RC of -45.7%
	N1	NC (↓)			
	N2	↓			
13	T	↓		Yes	
	N	↓			
18	T	NC (↓)		No (but equivocal)	N reduced HV_{MRI} at W2 T hypoxia decrease of 43.1% approached the RC of -45.7%
	N	↓			
19	T	NC	↓	Yes	
	N	NC	↓		
20	T	NC	NC	No	T hypoxia increased 59.7% at W4 whereas N reduced HV_{MRI}; neither lesion changed at W2
	N	NC	↓		
21	T	↓	↓	Yes	
	N	↓	↓		
23	T	NC		Yes	
	N	NC			
29	T	↓	↓	No (at W2) Yes (at W4)	Concordance does not manifest until W4
	N	NC	↓		
31	T		↓	Yes	
	N		↓		
35	T	↓	↓	Yes	
	N	↓	↓		
37	T	↓		No	T had reduced HV_{MRI} at W2, but N did not
	N	NC	↓		

Table 3*: Evaluation of concordance of hypoxia modification in patients with two or more lesions, by assessing serial values of HV_{MRI} at pre-treatment and W2 and W4. If HVMRI was reduced beyond the RC of -45.7% then HVMRI for that lesion is reduced (↓) otherwise there is no change (NC) measured.*